Title: A novel approach for automatic whisker tracking in head-restrained rodents from high-speed videos

Authors: Diego L. Guarin, PhD[1]; Christopher J. Knox B.S.[1]; Tessa A. Hadlock[1], MD; and Nate Jowett, MD[1]

[1] Department of Otolaryngology/Head and Neck Surgery, Massachusetts Eye and Ear Infirmary and Harvard Medical School, 243 Charles St, Boston, MA 02114, USA

Corresponding Author:

Diego L. Guarin, PhD

Massachusetts Eye and Ear Infirmary

243 Charles Street, 02114, Boston, MA, USA

diego_guarin@meei.harvard.edu

Tel: 617-573-3837

Fax: 617-573-3727

Abstract word count: 249

Manuscript word count: 4409

Abstract

Background: Tracking movement of rodent whiskers has important applications in the study of sensorimotor processing, integration and motor control. Herein we describe a new approach for automated tracking of whisker displacements from video, and provide source code and a Windows-based application.

New Method: High-speed videos (500 fps) were obtained of spontaneous free-air whisking behavior in head-restrained rats. Image analysis by iterative rotation of whisker regions between adjacent frames with subsequent identification of cross-correlation maxima was employed to determine the angular displacement of whisker arrays. Parallel processing was employed to minimize runtime.

Results: Excellent tracking accuracy was validated by comparison against manual markings. Free-air whisking was mostly cyclic and bilaterally synchronous, having a frequency bandwidth of 20Hz centered around 6Hz. Asynchronous movements were also observed, indicating that animals can move left and right whiskers independently. No significant difference in protraction and retraction amplitudes were observed; mean group values were $24.0^o \pm 7.31^o$ and $25.9^o \pm 8.84^o$ respectively ($p >> 0.01$). Significant differences in protraction and retraction durations were observed, mean group values were $57.7s \pm 11.7s$ and $102.6s \pm 16.37s$ respectively ($p << 0.01$).

Comparisons with Existing Methods: This approach obviates the need for manual whisker marking or trimming, which could impact whisking kinetics and behavior. By exploiting parallel processing capabilities of modern computers, this approach offers almost real-time whisker tracking over long video recordings.

Conclusions: We developed a novel digital image processing algorithm for offline tracking of whisker movements in head-restrained rodents during free-air whisking. The procedure was completely automated, and required no human intervention or supervision.

Keywords

Vibrissa (whisker) tracking; rodent; Motion Analysis; Image processing; parallel-processing

1. Introduction

Tracking rodent whisker movement has gained significant attention in recent years, as the vibrissal system has become one of the most common animal models for study of sensory-motor integration (Bush, Solla, & Hartmann, 2016; Diamond, Von Heimendahl, Knutsen, Kleinfeld, & Ahissar, 2008; Kurnikova, Moore, Liao, Deschênes, & Kleinfeld, 2017), neural representation (Houweling & Brecht, 2008; Moore, Lindsay, Deschênes, & Kleinfeld, 2015; Pinto, Brumberg, & Simons, 2000), and motor recovery following neural injury (Attiah, de Vries, Richardson, & Lucas, 2017; T. A. Hadlock, Heaton, Cheney, & Mackinnon, 2005; Heaton et al., 2008).

Early approaches to whisker movement tracking employed high-speed video recordings and manual marking of one or more whiskers in each individual video frame (Carvell, Simons, Lichtenstein, & Bryant, 1991; Mitchinson, Martin, Grant, & Prescott, 2007; Towal & Hartmann, 2006; Wineski, 1983). This procedure is error prone, and involves many hours of manual labor to trace only a few seconds of high-speed recordings (Voigts, Sakmann, & Celikel, 2008). Modern approaches for whisking tracking utilize automatic or semi-automatic procedures and can be broadly divided in two categories: marker- and markerless-based tracking.

Marker-based tracking systems employ specialized optoelectronic (Bermejo, Houben, & Zeigler, 1998), electromagnetic (Berg & Kleinfeld, 2003a), or high-speed videography (Szwed, Bagdasarian, & Ahissar, 2003) systems whose output is proportional to the position of a single whisker on each hemi-face. Optoelectronic systems use adhesive foam or polyamide whisker entubulation to generate a shadow within a laser emitter and detector array field into which the animals whiskers are positioned (Attiah et al., 2017; Gao, Bermejo, & Zeigler, 2001; Heaton et al., 2008; Hill, Bermejo, Zeigler, & Kleinfeld, 2008). Electromagnetic systems use a small magnet attached to the tip of one whisker, with vibrissae movement proportional to the change in

induced magnetoresistance within a magnetic field (Berg & Kleinfeld, 2003a). High-speed videography systems use small reflective markers (Berg & Kleinfeld, 2003b), or ink (Wallach, Bagdasarian, & Ahissar, 2016) to highlight one whisker and facilitate its automatic localization within each frame.

Marker-based whisking tracking systems offer high spatial and temporal resolution, enabling near real-time tracking of angular position and potential for closed-loop stimulation (Heaton, Knox, Malo, Kobler, & Hadlock, 2013; Wallach et al., 2016). Most marker-based approaches are limited to tracking the position of a single whisker on each side of the face. As rodents can move whiskers independently (Sachdev, Sato, & Ebner, 2002), tracking the position of a single whisker might fail to reflect the overall movement of the vibrissal array. Moreover, markers used to facilitate whisking tracking are often five to fifteen times heavier than the whisker to which they are attached (Heaton et al., 2008); such additional weight might impact displacement by altering whisking mechanics and behavior.

Markerless-based tracking systems employ high-speed cameras (500 frames/s or more) having high spatial resolution (VGA or higher) paired with specialized image processing algorithms to track whisker movements (Knutsen, Derdikman, & Ahissar, 2005). Though current markerless systems do not provide real-time estimates of whisker position, they permit assessment of unimpeded free-air whisking and unconstrained whisker-interactions with objects (Clack et al., 2012; O'Connor et al., 2010; Voigts et al., 2008). Previously reported algorithms for markerless whisker tracking were computationally expensive, requiring several hours to process each minute of high-speed video on conventional CPUs (Clack et al., 2012; Knutsen et al., 2005) and GPUs (Voigts et al., 2008). Furthermore, prior methods have necessitated whisker trimming such that only a single whisker or row of whiskers is left untrimmed to achieve accurate whisker

identification and localization (Clack et al., 2012; Kurnikova et al., 2017; Voigts et al., 2008). Such trimming effectively disables more than 90% of the animal's most important sensory organ (Diamond et al., 2008); the behavioral impact of whisker trimming has not been well characterized.

To avoid the need for whisking trimming, alternative markerless-based approaches have been developed. These methods compute the mean angular displacement of the entire whisker array on each side over time rather than tracking an individual whisker (Ebbesen, Doron, Lenschow, & Brecht, 2017; Towal & Hartmann, 2006). Such approaches markedly improve tracking efficiency by avoiding the need for frame-wise identification of individual whiskers.

Herein, we introduce a novel technique for free-air whisker tracking using high-speed video recordings of head-restrained rats. This method combines previously introduced and validated tracking algorithms into a single, multi-step approach that automatically and accurately tracks the angular displacement of right and left whisker arrays over time. The video processing algorithm requires no human intervention for initialization and processing. Moreover, the algorithm can process hundreds of frames per second through parallel processing, greatly reducing image processing times as compared to previously described markerless-based approaches to whisker tracking.

2. Materials and Methods

All procedures were approved by the Institutional Review Board. Three adult female Lewis rats (200 – 300 gram) were housed individually in a 12/h light-dark cycle with ad libitum food and water. Experiments were performed during light phase and animals were acclimatized to the experimental room for 30 minutes prior to recordings.

2.1. Head fixation and video recordings

Six weeks prior to behavioral testing, rats were fitted with a lightweight percutaneous titanium cranial implant that provided a set of four external attachment points for head fixation. Head implant design and surgical implantation procedures are described in detail elsewhere (T. Hadlock, Kowaleski, Mackinnon, & Heaton, 2007). During behavioral recordings of whisking activity, the animal's body was restrained using a soft cloth bag positioned within a polyvinyl chloride half pipe and secured using Velcro straps to prevent limb movement without restricting respiratory activity (Figure 1A). The animal's head was restrained by securing the titanium implant to four threaded posts with bolts (Figure 1B). Rats were conditioned to tolerate restraint for up to ten minutes.

A top-down view of the rodent face was recorded using a high-speed video camera (Figure 1E, Basler AG, Germany. Model acA800-510uc), fitted with a 6mm/F1.85 fixed focal length lens (Edmund Optics, USA. Part number 33301) at 500 frames/s; exposure time was limited to half of the duty cycle, corresponding to 1 ms of exposure per frame. The camera's field-of-view was adjusted such that all whiskers were included in each frame. Whisker visibility was enhanced by illuminating the recording area from below using a white LED array (Figure 1C, LIT Energy, USA), combined with white diffusing glass to obtain constant background illumination (Figure 1D, Edmund Optics, USA. Part number 34481). **Error! Reference source not found.**A presents a typical recorded frame, with the rostrocaudal midline indicated by a vertical line.

Two one-minute videos were recorded of free-air head-restrained whisking for each animal. Rats were presented with random auditory stimuli (clapping and cooing) to elicit fast, exploratory whisking behavior. Following video recordings, animals were immediately freed from their restraints and returned to their cages.

2.2 Image Processing

2.2.1 Initial conditions

The first step of the tracking algorithm comprised automatic specification of initial conditions from the first frame of a given video. The first condition involves localization of a fixed origin point in the rostrocaudal midline about which frame-wise angular rotations were performed. The second condition involves estimation of the initial angular position of right and left whisker array axes with respect to the coronal axis through the mid-snout. Knowledge of the initial angular positions of whisker array axes allows tracking of absolute angular displacements over time, when combined with frame-wise tracking of relative angular displacements in the second stage of the algorithm. Initial condition accuracy requires the eyes be open on the first frame, and tracking accuracy assumes the head remains in fixed position throughout the entire recording.

Origin point

An origin was automatically defined along the rostrocaudal midline near the center of the whisker arrays in the first frame of a given video using a multistep process. The facial contour was first determined using edge detection filtering after applying an 11 x 11 kernel dilation to eliminate fine details in the frame (Figure 2A). Gray-color thresholding was then applied to identify the darkest pixels within the facial boundaries, corresponding to the rodent eyes. A horizontal line was then plotted between the center of mass of each eye. The rostrocaudal midline was then defined as a line perpendicular to the interocular line at its mid-point (point *E* in Figure 2A), which intersects the facial contour near the tip of the snout (point *S* in Figure 2A) dividing it in roughly two equal parts. The origin (point *O* in Figure 2A) was then defined as a point one third the distance between the snout tip (point S) and the interocular midline (point E), roughly corresponding to the center region of the whisker pads along the rostrocaudal midline.

Initial whisker array angle

The initial angular positions of right (θ_R) and left (θ_L) whisker arrays were automatically determined for the initial frame of a given video. The whisker array axis was defined as a line that bisects the angle formed by lines connecting the most rostral and caudal whiskers to the origin on each side of the face (Figure 2B) (Towal & Hartmann, 2006). Left and right whisker array angles were then defined with reference to the coronal axis through the mid-snout (i.e., a line perpendicular to the rostrocaudal midline about the origin point O, cyan line in Figure 2). A multistep algorithm was employed for automatic calculation of initial angles. First, the facial contour was determined and image background removed by subtraction (Figure 2B). Gray-color thresholding was applied to extract pixels that might contain whisker signal. A circular region-of-interest (ROI) centered at the origin and having a diameter of 1.5x the distance between the origin (O) and the snout (S) was defined, pixels along the ROI located within the facial contour boundaries were discarded. The most rostral and caudal pixels containing whisker signal along the circumference of the circular ROI were identified on each side of the face. The presence of whisker signal was determined by selecting a 7x7 region centered about each pixel along the circular ROI, and validating whether the location of intensity maxima along each row or column conformed to a line (O'Connor et al., 2010).

2.2.2 Tracking whisker movements

With initial angular positions defined, frame-to-frame angular displacements of right and left whisker arrays were then tracked. Iterative rotation of whisker regions between adjacent frames with subsequent identification of the cross-correlation maxima was employed to determine the mean angular displacement of whisker arrays over time as proposed by Ebbesen et al. (Ebbesen et al., 2017). First, each frame was divided in two about the rostrocaudal midline. Relative

angular displacements of right and left whiskers arrays between successive frames was then determined in frame-wise fashion as follows. Two adjacent frames were selected, backgrounds were subtracted, and the intensity of pixels located within facial contour boundaries were set to zero,; this procedure resulted in new images where only whiskers and facial boundaries remain (Figure 3A and B). Cross-correlation of adjacent frames was then performed over a user-defined range of possible rotation angles of one frame relative to the other about the origin (Figure 3C). This procedure was repeated for all pairs of adjacent frames in a video for the right and left side of the face, generating a time-series of estimated whisker array axis angular positions when combined with initial conditions (Figure 3D).

As a rotation angle was obtained for each pair of consecutive frames, parallel-processing with M processors was used to analyze the N frames of video. This was achieved by splitting N frames of video into M subgroups each containing $\lfloor N/M \rfloor$ +1 frames. Initial conditions were estimated only for the first frame of the video in the first subgroup; remaining subgroups used the same origin and only relative angular displacements between adjacent frames was computed. Once all subgroups were processed, the last angular rotation of each subgroup was removed and assigned as the initial condition of the following subgroup. Finally, results were concatenated to form an N-point time series.

A high performance workstation PC was used for image processing (Genesis II, Puget Systems, Auburn, WA), comprising dual twelve core processors (Xeon E5-2687W V4, 3.0 GHz, Intel), 256 MB RAM (8 x 32 GB, DDR4-2133, Samsung), and a 2TB SATA SSD hard drive (EVO 850, Samsung).

2.3 Data Analysis

Whisker array axis angular displacement signals were post-processed by applying a low-pass filter (125 Hz cut-off frequency) to remove high-frequency noise, followed by numerical integration to compute the overall displacement of the whiskers array as a function of time, and high-pass filtering (1 Hz cut-off frequency) to remove any low-frequency drifts added by the numerical integration procedure (Figure 3E).

Overall whisker array axis displacements were analyzed in the time-domain by computing array protraction (caudal-rostral movement) and retraction (rostral-caudal movement) amplitudes and durations. Protractions were defined as displacements occurring between local angular minima and maxima, and retractions defined as the opposite. Signals were also analyzed in the frequency-domain by computing the power spectrum using Matlab (MathWorks) *spectrogram* function. A signal's power spectrum illustrates how its power is distributed as a function of frequency.

2.4 Validation

Algorithm results were validated by comparison against manual estimation of right-sided whisker array angles for a 1000 frame-length video sequence. Using a custom-designed graphical user interface, two trained volunteers independently selected the intersections of a circular ROI (Figure 2B) with the most rostral and caudal whiskers for each frame. Origin and ROI radius was the same for manual and automatic whisker tracking. Whisker array axis angles were calculated as described above, and results were averaged between volunteers.

Manual and automatic estimates of whisker array angles were compared by calculation of the Variance Accounted For (%VAF) between them. The %VAF is given by

$$\%VAF = \left[1 - \frac{\sum(y_m(t) - y_a(t))^2}{\sum(y_m(t))^2}\right] \times 100\%$$

where $y_m(t)$ and $y_a(t)$ are the time-series of manual and automated whisker angular displacement estimates. The %VAF measures how well the automatic results ($y_a(t)$) explain the variability present in the manual results ($y_m(t)$), thus providing an objective and quantifiable measure of the agreement between both signals.

2.5 Influence of algorithm parameters

There are multiple algorithm parameters that might influence the tracking results, such as the origin position, angular range, and angular resolution used to estimate whisker array rotation between consecutive frames. The impact of variation of these parameters over reasonable ranges on whisker array axis tracking was characterized to validate the robustness of the present algorithm to parameters variation.

3. Results

3.1 Validation

Figure 4 illustrates that the algorithm's output closely followed manually-tracked whisker array axis displacements; a %VAF of 98.4% confirmed high agreement between the two measures. The largest difference between manual and automatic results was observed when the whiskers reached their most caudal position (between frames 700 and 1000 in Figure 4).

3.2 Influence of algorithm parameters

Selection of origin point

Variation in the origin position about the snout resulted in minimal changes in whisker array axis tracking. Figure 5 demonstrates the location of nine different origin positions tested, together

with their respective outputs from the tracking algorithm for the right whisker array axis. Positions tested included the automatic algorithm-defined origin (B2 in Figure 5), and eight manually selected positions about and lateral to the rostrocaudal midline axis. Excellent correlation of the nine outputs was observed, with the only notable difference between signals being the baseline initial angular position of the whisker array axis. High agreement between the nine outputs was confirmed by computing the %VAF between algorithm-defined origin and each of the eight manually selected deviated origins; VAFs exceeded 98% for all tested locations (Table 1).

Angular range

Table 2 presents a comparison of %VAFs obtained with different angular ranges for frame rotations in computing cross-correlation maxima in comparison to results obtained with a large angular range $\pm 10°$. Results indicate that decreasing the angular range to $\pm 3°$ had minimal effect on the tracking results. However, further decreasing the angular range produced whisker tracking results very different from those obtained with larger ranges, indicating that the angular rotation between frames were not properly captured when the angular range was smaller than $\pm 3°$.

Number of angles

Table 3 presents the results obtained by modifying the number of angular rotations when processing 10000 video frames, with columns presenting the number of angles used, processing time, estimated number of frames processed each second, and the %VAF computed in comparison to results obtained using 100 angles. Here, the %VAF is averaged between results obtained for right and left sides. Results indicate that reducing the number of angles had a major impact in the processing time; the processing time decreased linearly as a function of the number

of angles (Pearson's linear correlation coefficient = 0.99, $p < 0.01$). In contrast, the accuracy of whisker tracking was largely unaffected by a steep reduction in the number of tested angles up to a specific threshold. Halving the number of tested angles provided nearly identical tracking results, while halving processing time. Use of 12 angular steps resulted in minimal impact on tracking accuracy while enabling near real-time tracking (492.1 frames processed per second). Further reduction in the number of angular rotations negatively influenced tracking accuracy.

3.3 Whisking Behavioral Results

Figure 6 presents a tracing that describes average whisking motion during10 seconds of whisker tracking in three animals. Mean values were removed to facilitate comparison between sides and subjects. Most often, left and right whisker array axes moved in synchrony. Asynchronous movements were also seen, where arrays moved in opposite directions, or movement of one array occurred without movement of the other. This behavior was observed in all animals, as demonstrated by the shaded areas in Figure 6.

Figure 7 presents the power spectra for right and left whisker array axis displacements for all subjects. Power spectra were computed by splitting the two one-minute recordings into ten-second windows. Whisker array axes moved with a frequency bandwidth limited to 20 Hz, centered around 6Hz, with an additional prominent peak around 2 Hz, in agreement with previously published findings (Gao et al., 2001; Hill et al., 2008; Jin, Witzemann, & Brecht, 2004). Finally, Table 4 presents whisker array axis protraction (caudal-rostral movement) and retraction (rostral-caudal movement) duration and amplitude. Whisker protraction was significantly slower than retraction within subjects ($p \ll 0.01$); without any differences noted in the amplitudes of protraction and retraction movements within subjects ($p \gg 0.01$). Moreover, protraction and retraction durations were not significantly different within subjects ($p \gg 0.01$).

Finally, we observed no linear correlation between protraction amplitude and duration (group results: Pearson's linear correlation coefficient = -0.034, $p = 0.76$), and retraction amplitude and duration (group results: Pearson's linear correlation coefficient = 0.088, $p = 0.41$).

4. Discussion and Conclusions

We developed a novel digital image processing algorithm for offline tracking of whisker movements in head-restrained rodents during free-air whisking. The procedure was completely automated, and required no human intervention or supervision. Automatic tracking results were remarkably similar to manually estimated whisker array displacements, with discrepancies occurring only where whisker arrays reached their most caudal position. In this position, whisker localization becomes challenging due to overlap with the facial boundaries and facial fur. Despite this limitation, manual tracking corresponded to automatic tracking to an exceptionally high degree, thus validating the algorithm's ability to accurately track whisker array movements from high-speed videos.

Moreover, we found the novel algorithm to be robust to changes in algorithm parameters, such as origin position, angular range, and number of angles tested within the angular range. Results demonstrated that placing the origin at different positions about the snout yielded similar tracking results; only the initial positions of the whisker array axes were noted to be highly dependent on origin positioning. Determination of the initial position of whisker array axes is important for comparison of left and right whisking behavior, and for group studies. Estimation of initial array positions was addressed through automated placement of an origin point along the rostrocaudal midline in the center region of the snout.

The method developed herein was found to be robust to angular range and resolution changes up to specific thresholds in determining cross-correlation maxima of iterative rotations of adjacent frames. Changes in angular range from $\pm 10°$ to $\pm 3°$ yielded minimal differences in tracking results. Similarly, tracking accuracy was largely unaffected by a steep reduction in the number of steps within the angular range; a reduction from 100 to 6 angles yielded a VAF larger than 90%. A large reduction in tracking accuracy was noted when the angular range was set below ± 3°, indicating this was the smallest range within which all possible array displacements between successive frames could be captured with this experimental setup. The appropriate angular range is dependent on the frame rate of the video camera, and animal-dependent speed of whisker displacements; slower frame rates would necessitate larger angular ranges, as larger displacements may occur during the longer time lapses between frames. Likewise, larger ranges may be required for smaller rodents, who demonstrate higher whisker array peak angular velocities (Jin et al., 2004).

Whisking behavioral trends observed using our algorithm were similar to those previously reported using alternative approaches for whisker tracking. In general, whisking was near cyclic and predominantly synchronous between sides. Short episodes of asynchronous whisking were often noted, indicating that rats can independently control mystacial vibrissae movements on both sides of the face. Despite having a broad peak around 6 Hz, no single sharp peak whisking frequency nor group of frequencies was observed, as one might expect from a periodic movement. The absence of a peak whisking frequency suggests that rat whisking is non-periodic, that animals actively modify whisking frequency during movements, or both (Gao et al., 2001; Hill et al., 2008; Towal & Hartmann, 2006).

Finally, the lack of linear correlation between retraction amplitudes and durations indicates that these movements may be produced by active contraction of antagonist muscles, contrary to a passive, spring-like movement. These results challenge the classical perception that whisker retraction is a passive process induced by the viscoelastic properties of the skin and muscle (Dörfl, 1982), and reinforce the experimental finding that whisking protraction and retraction are under active muscular control (Berg & Kleinfeld, 2003a; Hill et al., 2008).

4.1 Comparison with other methods

Our approach possesses four important advantages over other methods: first, it does not require the addition of a marker that might modify the mechanical properties of the whisker to which it is attached. Second, the approach does not require specialized, expensive, custom-assembled equipment, and associated cumbersome calibration steps. Herein, we used a commercially-available, miniature, high-resolution, and low-cost high speed camera for data acquisition. In addition to its own user-friendly graphical user interface, the camera used herein has freely available drivers for device control within popular programming ecosystems including MATLAB and Python. Importantly, other facial signals such as blink and ear displacements could be concurrently tracked from the same frames, obviating the need for separate hardware and synchronization steps for multi-facial parameter tracking. Third, this method does not require trimming of whiskers. Having multiple long whiskers available in the field of view is expected to increase algorithm robustness, as more content is available to compute the cross-correlation between frames. Moreover, there is experimental evidence that whisker trimming in neonatal rodents leads to permanent abnormalities in cortical anatomy (Mitchinson et al., 2007), and that trimming of whiskers in adult rats leads to significant changes in cortical activity (Kelly, Carvell, Kodger, & Simons, 1999). It is thus possible that rodents might exhibit abnormal

whisking patterns following whisker trimming. Finally, previously introduced image analysis approaches for whisker tracking report processing times on the order of one frame per second (Clack et al., 2012; Knutsen et al., 2005; O'Connor et al., 2010; Voigts et al., 2008). These approaches required several hours for processing a few minutes of video recorded at 500 fps. In contrast, our approach takes advantage of parallel processing techniques on a modern 24-core processor computer, achieving a near real-time processing rate close to 500 frames per second. Future implementations of this algorithm could make use of parallel processing techniques using modern graphical processing units having hundreds of cores, which would further reduce processing times.

Limitations

This whisking tracking approach possesses important limitations. Rodents must be head restrained and the camera must have an unrestricted view of the whiskers. Consequently, this approach cannot be used to track whiskers in unrestrained behaving rodents. However, behavioral studies of whisking in unrestrained animals are challenging due to lack of control over exafferent inputs (Gao et al., 2001). As a result, the majority of behavioral studies typically employ head restraint to enable control of sensory inputs; such restraint would make use of this algorithm readily feasible by other groups.

In contrast to other approaches, this algorithm cannot be used to track individual whiskers, nor can it be used to track whisker deformation during object contact. Though tracking of whisker deformation has been used to estimate the force produced at the sensory follicle for studies of sensory motor integration (Clack et al., 2012; O'Connor et al., 2010; Voigts et al., 2008), recent work has called this approach into question. Simulation studies have demonstrated that the level of tracking accuracy required to estimate the force produced at each follicle due to whisker

deformation is not yet attainable by any available method, and that more advanced three-dimensional measurements may be required to fully characterize vibrissae kinematics and dynamics (Bush et al., 2016; Knutsen, Biess, & Ahissar, 2008; Yan, Graff, & Hartmann, 2016).

Finally, current implementation of the algorithm does not produce real-time estimates of whiskers position, and thus cannot be used as part of an online functional stimulation system.

4.2 Availability

Source code and documentation for Python implementation or our algorithm are freely available online (github.com/dguari1); source code is based on open-source libraries and toolkits (Open CV and PyQt), and can be executed on multiple platforms (Windows, OS X, and Linux). We also provide a pre-compiled Windows application with a user-friendly graphical user interface (GUI) that facilitates selection of user-defined parameters. The GUI also includes options to remove the image background, and reproduce the video at different playback speeds. Finally, the provided software greatly simplifies the manual marking procedure, facilitating the creation of validation data sets.

4.3 Conclusions

We developed an image-processing approach for offline tracking of whisker array displacements in head-restrained rodents, complete with a GUI and example videos for rapid implementation across other centers. The algorithm performs automatic tracking and requires no human intervention or supervision. This method may prove useful for whisker movement analysis and rodent behavioral research by facilitating analysis of long data sets using readily available equipment.

6. Acknowledgments

This work was supported by NIH grant number 2R01NS071067-06A1 and the Berthiaume Family Foundation. DLG was supported by the Fonds Qubecoise de Recherche Nature et Technologies, grant number 208637.

7. References

Attiah, M. A., de Vries, J., Richardson, A. G., & Lucas, T. H. (2017). A Rodent Model of Dynamic Facial Reanimation Using Functional Electrical Stimulation. *Frontiers in neuroscience, 11*, 193.

Berg, R. W., & Kleinfeld, D. (2003a). Rhythmic whisking by rat: retraction as well as protraction of the vibrissae is under active muscular control. *Journal of neurophysiology, 89*(1), 104-117.

Berg, R. W., & Kleinfeld, D. (2003b). Vibrissa movement elicited by rhythmic electrical microstimulation to motor cortex in the aroused rat mimics exploratory whisking. *Journal of neurophysiology, 90*(5), 2950-2963.

Bermejo, R., Houben, D., & Zeigler, H. P. (1998). Optoelectronic monitoring of individual whisker movements in rats. *Journal of neuroscience methods, 83*(2), 89-96.

Bush, N. E., Solla, S. A., & Hartmann, M. J. (2016). Whisking mechanics and active sensing. *Curr Opin Neurobiol, 40*, 178-188. doi:10.1016/j.conb.2016.08.001

Carvell, G. E., Simons, D. J., Lichtenstein, S. H., & Bryant, P. (1991). Electromyographic activity of mystacial pad musculature during whisking behavior in the rat. *Somatosensory & motor research, 8*(2), 159-164.

Clack, N. G., O'Connor, D. H., Huber, D., Petreanu, L., Hires, A., Peron, S., . . . Myers, E. W. (2012). Automated tracking of whiskers in videos of head fixed rodents. *PLoS computational biology, 8*(7), e1002591.

Diamond, M. E., Von Heimendahl, M., Knutsen, P. M., Kleinfeld, D., & Ahissar, E. (2008). 'Where'and'what'in the whisker sensorimotor system. *Nature Reviews Neuroscience, 9*(8), 601.

Dörfl, J. (1982). The musculature of the mystacial vibrissae of the white mouse. *Journal of anatomy, 135*(Pt 1), 147.

Ebbesen, C. L., Doron, G., Lenschow, C., & Brecht, M. (2017). Vibrissa motor cortex activity suppresses contralateral whisking behavior. *Nature neuroscience, 20*(1), 82.

Gao, P., Bermejo, R., & Zeigler, H. P. (2001). Whisker deafferentation and rodent whisking patterns: behavioral evidence for a central pattern generator. *Journal of Neuroscience, 21*(14), 5374-5380.

Hadlock, T., Kowaleski, J., Mackinnon, S., & Heaton, J. T. (2007). A novel method of head fixation for the study of rodent facial function. *Experimental neurology, 205*(1), 279-282.

Hadlock, T. A., Heaton, J., Cheney, M., & Mackinnon, S. E. (2005). Functional recovery after facial and sciatic nerve crush injury in the rat. *Archives of facial plastic surgery, 7*(1), 17-20.

Heaton, J. T., Knox, C. J., Malo, J. S., Kobler, J. B., & Hadlock, T. A. (2013). A system for delivering mechanical stimulation and robot-assisted therapy to the rat whisker pad during facial nerve regeneration. *IEEE Transactions on Neural Systems and Rehabilitation Engineering, 21*(6), 928-937.

Heaton, J. T., Kowaleski, J. M., Bermejo, R., Zeigler, H. P., Ahlgren, D. J., & Hadlock, T. A. (2008). A system for studying facial nerve function in rats through simultaneous bilateral monitoring of eyelid and whisker movements. *Journal of neuroscience methods, 171*(2), 197-206.

Hill, D. N., Bermejo, R., Zeigler, H. P., & Kleinfeld, D. (2008). Biomechanics of the vibrissa motor plant in rat: rhythmic whisking consists of triphasic neuromuscular activity. *Journal of Neuroscience, 28*(13), 3438-3455.

Houweling, A. R., & Brecht, M. (2008). Behavioural report of single neuron stimulation in somatosensory cortex. *Nature, 451*(7174), 65-68. doi:10.1038/nature06447

Jin, T.-E., Witzemann, V., & Brecht, M. (2004). Fiber types of the intrinsic whisker muscle and whisking behavior. *Journal of Neuroscience, 24*(13), 3386-3393.

Kelly, M. K., Carvell, G. E., Kodger, J. M., & Simons, D. J. (1999). Sensory loss by selected whisker removal produces immediate disinhibition in the somatosensory cortex of behaving rats. *Journal of Neuroscience, 19*(20), 9117-9125.

Knutsen, P. M., Biess, A., & Ahissar, E. (2008). Vibrissal kinematics in 3D: tight coupling of azimuth, elevation, and torsion across different whisking modes. *Neuron, 59*(1), 35-42.

Knutsen, P. M., Derdikman, D., & Ahissar, E. (2005). Tracking whisker and head movements in unrestrained behaving rodents. *Journal of neurophysiology, 93*(4), 2294-2301.

Kurnikova, A., Moore, J. D., Liao, S.-M., Deschênes, M., & Kleinfeld, D. (2017). Coordination of orofacial motor actions into exploratory behavior by rat. *Current Biology, 27*(5), 688-696.

Mitchinson, B., Martin, C. J., Grant, R. A., & Prescott, T. J. (2007). Feedback control in active sensing: rat exploratory whisking is modulated by environmental contact. *Proceedings of the Royal Society of London B: Biological Sciences, 274*(1613), 1035-1041.

Moore, J. D., Lindsay, N. M., Deschênes, M., & Kleinfeld, D. (2015). Vibrissa self-motion and touch are reliably encoded along the same somatosensory pathway from brainstem through thalamus. *PLoS biology, 13*(9), e1002253.

O'Connor, D. H., Clack, N. G., Huber, D., Komiyama, T., Myers, E. W., & Svoboda, K. (2010). Vibrissa-based object localization in head-fixed mice. *Journal of Neuroscience, 30*(5), 1947-1967.

Pinto, D. J., Brumberg, J. C., & Simons, D. J. (2000). Circuit dynamics and coding strategies in rodent somatosensory cortex. *Journal of neurophysiology, 83*(3), 1158-1166.

Sachdev, R. N., Sato, T., & Ebner, F. F. (2002). Divergent movement of adjacent whiskers. *Journal of neurophysiology, 87*(3), 1440-1448.

Szwed, M., Bagdasarian, K., & Ahissar, E. (2003). Encoding of vibrissal active touch. *Neuron, 40*(3), 621-630.

Towal, R. B., & Hartmann, M. J. (2006). Right–left asymmetries in the whisking behavior of rats anticipate head movements. *Journal of Neuroscience, 26*(34), 8838-8846.

Voigts, J., Sakmann, B., & Celikel, T. (2008). Unsupervised whisker tracking in unrestrained behaving animals. *Journal of neurophysiology, 100*(1), 504-515.

Wallach, A., Bagdasarian, K., & Ahissar, E. (2016). On-going computation of whisking phase by mechanoreceptors. *Nature neuroscience, 19*(3), 487.

Wineski, L. E. (1983). Movements of the cranial vibrissae in the golden hamster (Mesocricetus auratus). *Journal of Zoology, 200*(2), 261-280.

Yan, S., Graff, M. M., & Hartmann, M. J. (2016). Mechanical responses of rat vibrissae to airflow. *Journal of Experimental Biology, 219*(7), 937-948.

Figures:

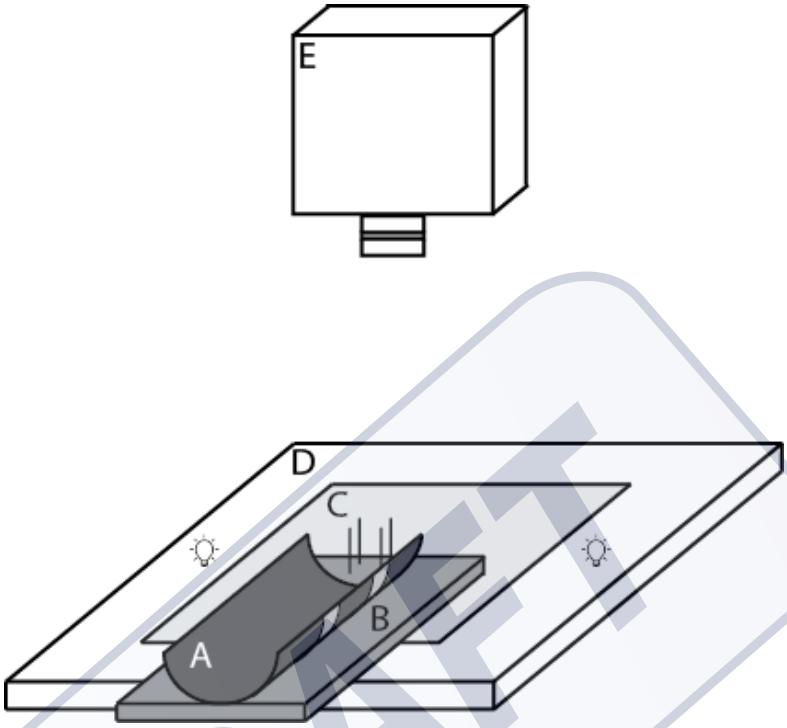

Figure 1. (A & B) Rodent rigid restraint and head fixation device. Video recording apparatus, comprised of diffusion glass (C), LED backlight (D), and high-speed camera (E).

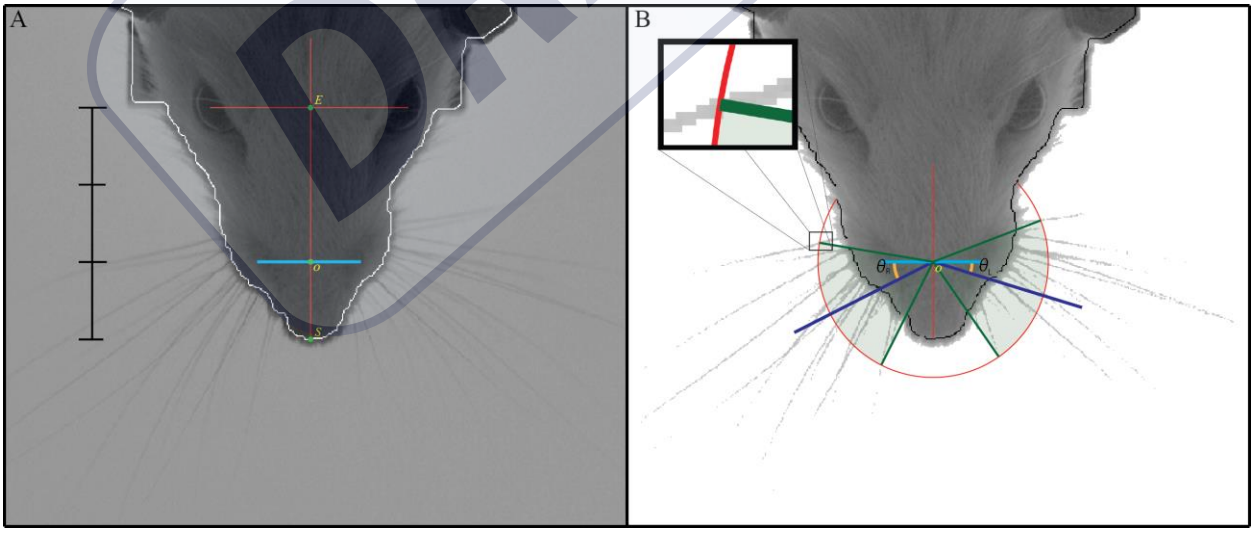

Figure 2. Estimation of whisker array axis angles. A) Original video frame displaying the automatically defined interocular midpoint (E), snout midpoint (S) and origin position (O). The origin is located along the rostrocaudal midline (E-S line) at 1/3 of the distance between the snout and the interocular midpoint. B) Processed video frame displaying a circular region-of-interest about the origin (O) with identification of most rostral and caudal whiskers along the circumference. Right and left whisker array axes (dark blue lines) are defined as a line bisecting the angle formed by two lines connecting the most rostral and caudal whiskers to the origin on each side of the face (green lines). Right (θ_r) and left (θ_l) whisker array axis angles are then defined with respect to the coronal axis (light blue line) passing through the origin, perpendicular to the rostrocaudal midline.

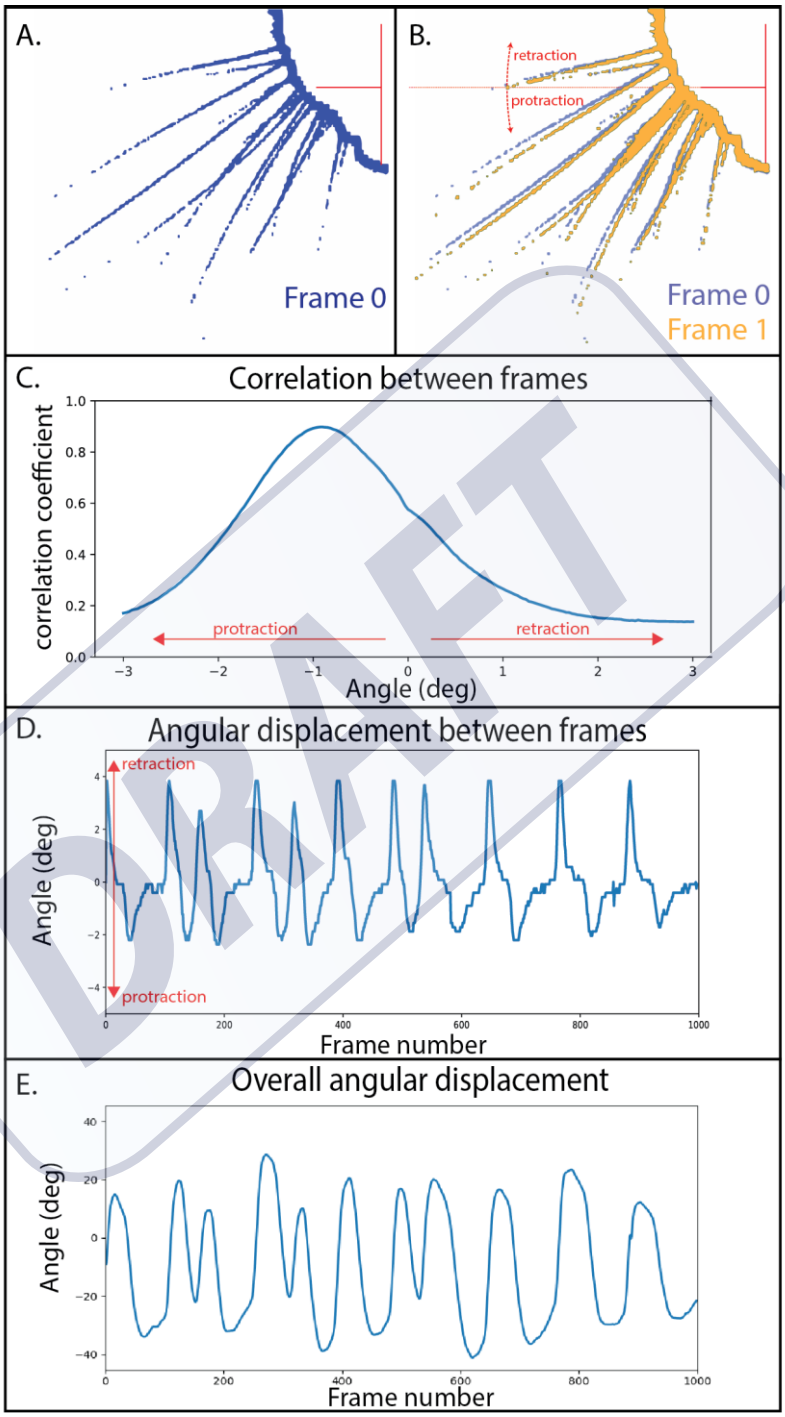

Figure 3. Estimation of whisker array angular rotation between adjacent frames. (A and B) Example of two adjacent frames, protraction and retraction directions are indicated, panel B shows frame 1(yellow) superimposed on frame 0 (blue) highlighting the whiskers movement between frames. C) Correlation coefficient between Frame 0 and a rotated version of Frame 1, 100 rotations were performed around the origin between -3^0(protraction) and 3^o(retraction). Correlation between Frame 0 and Frame 1 was largest at -0.96^o, indicating that the mystacial vibrissae moved slightly towards the protraction direction between frames. D) Angular displacement estimated for 1000 frames, and E) overall angular displacement obtain after post-processing the angular displacement signal.

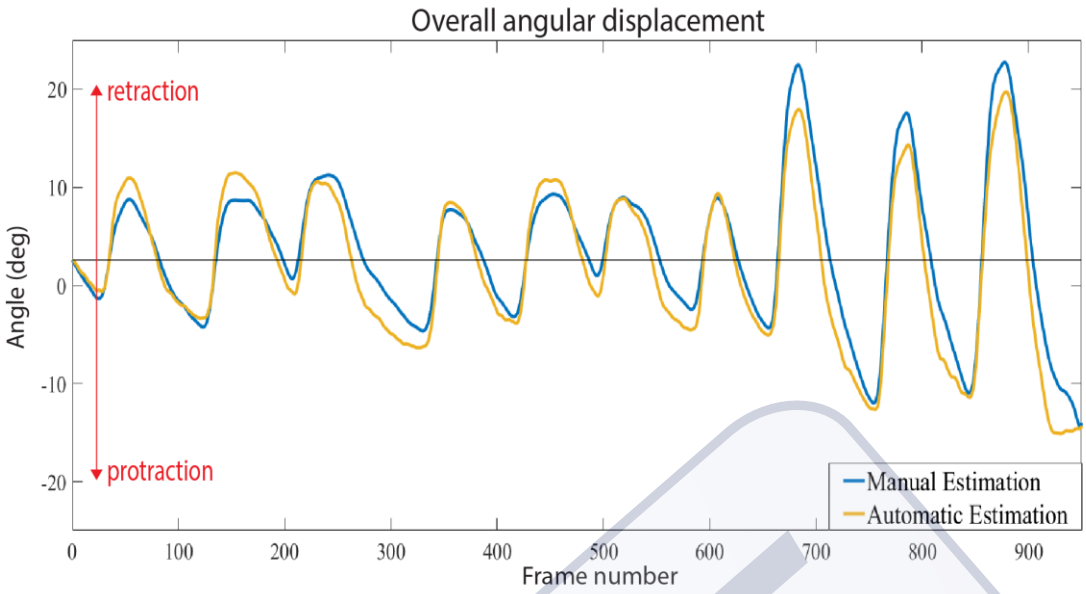

Figure 4. Comparision of whisker array axis movement obtained using manual (blue) and automatic (yellow) whisker tracking procedures. Automatic tracking was performed with an angular range of -4 to 4 degress with 100 steps within the angular range. The same origin position was used for manual and automatic whisker tracking. Excellent agrement between manual and automatic results was demonstrated by a VAF of 98.4%.

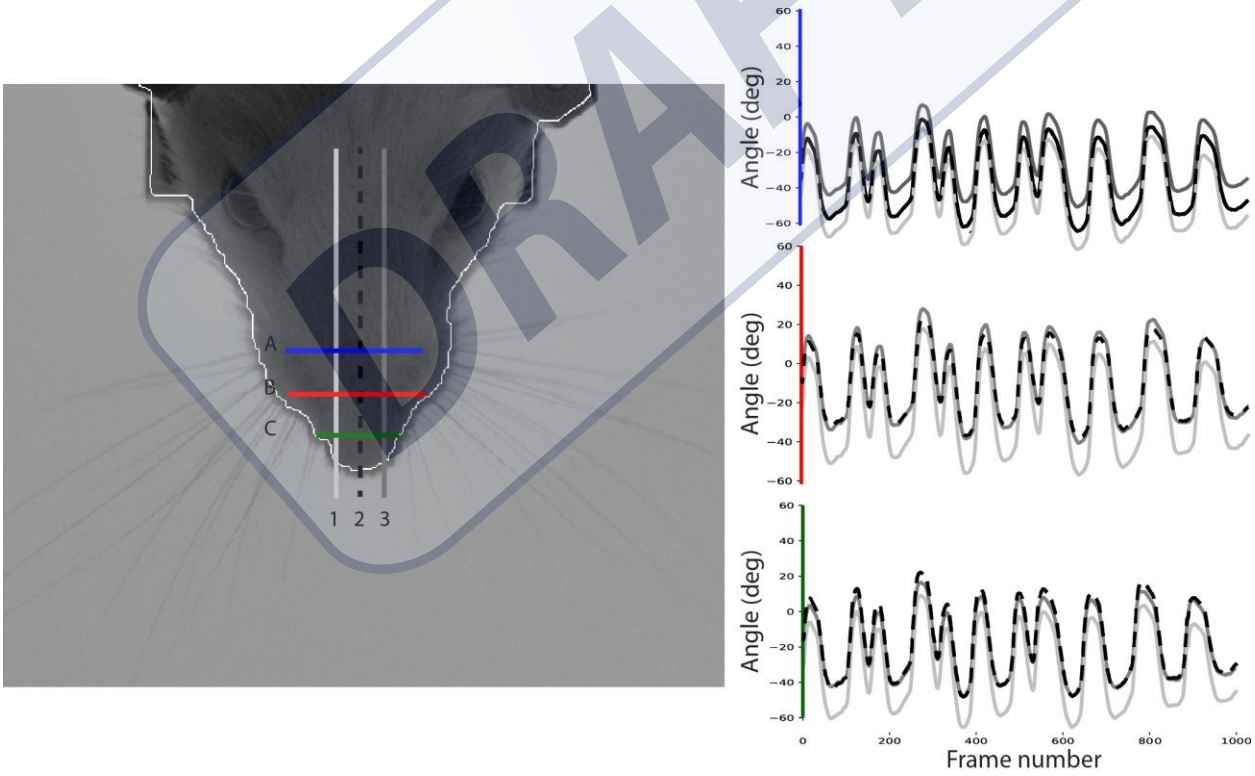

Figure 5. Automatic right-sided whisking array axis tracking results obtained for different origin positions. Left Column - Typical frame showing the nine different locations selected as origin, these locations were selected by translating the origin along the rostrocaudal midline and to the left and right of the midline. The selected positions where three caudal (A1, A2 and A3), three rostral (C1, C2 and C3) and three along the middle of the whisker pad (B1, B2 and B3). Optimal origin (center of the whisker pad along the rostrocaudal midline) corresponds to position B2. Right Column - Right whisker array axis displacement obtained by changing the origin position, results are color coded according to the origin location. Whisker array axis baseline position varied according to origin position; however, relative whisker displacements were almost identical

for all origin positions tested. Results were obtained using an angular range between ±4° with 100 steps in assessing cross-correlation maxima between successive frames.

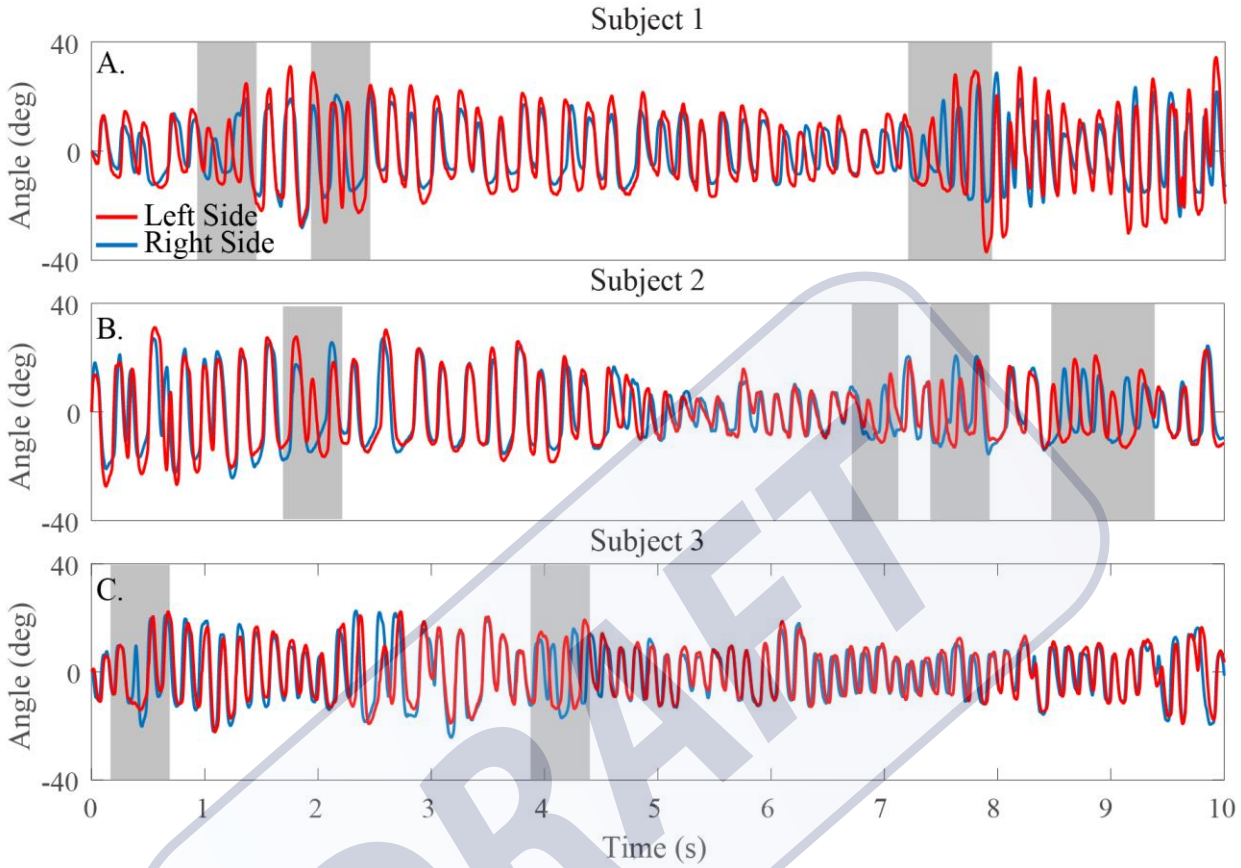

Figure 6. Whisker array axis angluar displacements for the left- (red) and right- (blue) sides for 3 different recording subjects as a function of time. Highlighted areas indicate the episodes of bilateral asynchronous movement. Results were obtained using an angular range between ±4° with 100 steps in assessing cross-correlation maxima between successive frames.

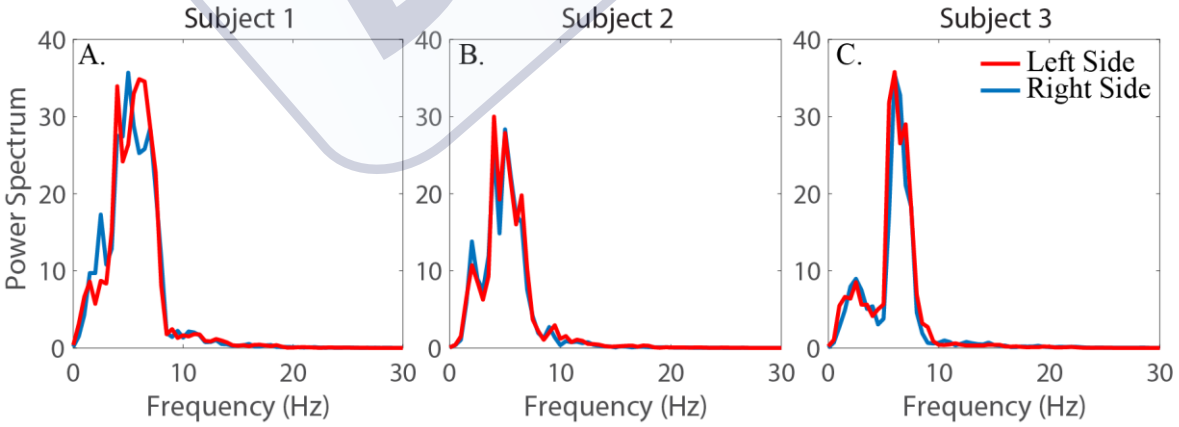

Figure 7. Power spectrum analysis between left- (red) and right- (blue) whiskers array axis angular displacements for 3 different recording subjects

Tables:

Table 1. Tracking results obtained by modifying the origin position. All tested positions were compared against the optimal position provided by the automatic procedure described herein (B2). Changing origin position had minimal effects on tracking results as demonstrated by the high %VAF.

	1	*2*	*3*
A	99.5%	99.5%	98.5%
B	99.0%	100%	99.0%
C	98.1%	99.7%	99.7%

Table 2. Whisker array axis tracking results obtained by modifying the angular range in assessing cross-correlation maxima between successive frames. All tested angular ranges were compared against the largest angular range ($[-10°,\ 10°]$). Modification of angular range had minimal effects on tracking accuracy up to certain limit ($([-3°,\ 3°]$ in this case). Below this limit, tracking accuracy was drastically reduced indicating that angular displacements of whisker arrays between consecutive frames was sometimes greater than the selected range.

Angular Range (degrees)	*%VAF*
[-10, 10]	100%
[-9, 9]	99.9%
[-8, 8]	99.9%
[-7, 7]	99.9%
[-6, 6]	99.9%
[-5, 5]	99.9%
[-4, 4]	99.9%
[-3, 3]	98.7%
[-2, 2]	85.9%
[-1, 1]	69.3%

Table 3: Whisker array axis tracking results obtained by modifying the number of angles tested whithin a fixed angular range of $\pm 4°$ in assessing cross-correlation maxima between successive frames. All tested values were compared agains results obtained with 100 angles. Reducing the number of rotations had a significant effect in the processing time of 10000 frames (second column), but reduced only slightly the tracking accuracy (fourth column).

Number of angles within fixed angular range	*Processing time (s)*	*Frames processed per second*	*%VAF*
100	129.06	77.5	100%
75	83.10	120.4	99.9%
50	59.65	167.6	99.9%
25	31.04	322.2	99.3%
12	20.31	492.1	98.8%
6	13.49	741.3	90.4%

Table 4. Retraction and protraction duration and amplitude computed from videos recorded of three subjects.

	Retraction Duration (ms)	*Protraction Duration (ms)*	*Retraction Amplitude (deg)*	*Protraction Amplitude (deg)*
Subject 1	58.4 ± 12.4	101.6 ± 19.3	32.13 ± 10.19	32.28 ± 11.01
Subject 2	57.7 ± 10.8	106.3 ± 16.2	20.46 ± 5.83	24.28 ± 8.68
Subject 3	57.0 ± 11.9	99.9 ± 14.8	19.54 ± 5.88	21.38 ± 6.84